THE JOURNAL OF PHYSICAL CHEMISTRY LETTERS
A JOURNAL OF THE AMERICAN CHEMICAL SOCIETY

pubs.acs.org/JPCL

Perspective

Nonadiabatic Excited-State Molecular Dynamics Methodologies: Comparison and Convergence

Victor M. Freixas, Alexander J. White, Tammie Nelson, Huajing Song, Dmitry V. Makhov, Dmitrii Shalashilin, Sebastian Fernandez-Alberti,* and Sergei Tretiak*

Cite This: *J. Phys. Chem. Lett.* 2021, 12, 2970−2982

Read Online

ACCESS | Metrics & More | Article Recommendations | Supporting Information

ABSTRACT: Direct atomistic simulation of nonadiabatic molecular dynamics is a challenging goal that allows important insights into fundamental physical phenomena. A variety of frameworks, ranging from fully quantum treatment of nuclei to semiclassical and mixed quantum−classical approaches, were developed. These algorithms are then coupled to specific electronic structure techniques. Such diversity and lack of standardized implementation make it difficult to compare the performance of different methodologies when treating realistic systems. Here, we compare three popular methods for large chromophores: Ehrenfest, surface hopping, and multiconfigurational Ehrenfest with *ab initio* multiple cloning (MCE-AIMC). These approaches are implemented in the NEXMD software, which features a common computational chemistry model. The resulting comparisons reveal the method performance for population relaxation and coherent vibronic dynamics. Finally, we study the numerical convergence of MCE-AIMC algorithms by considering the number of trajectories, cloning thresholds, and Gaussian wavepacket width. Our results provide helpful reference data for selecting an optimal methodology for simulating excited-state molecular dynamics.

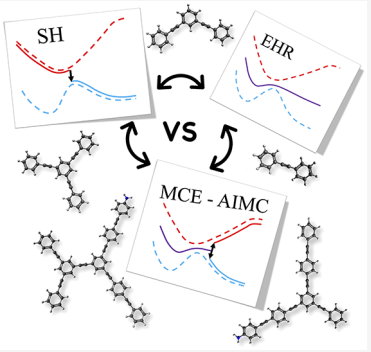

The dynamics of electronic excitations, such as charge (electrons and holes) and energy (excitons) carriers, lies at the heart of many applications, including light harvesting,[1] lighting,[2] catalysis,[3] detection, and sensing,[4] across a broad range of molecular and solid-state materials. There exist a variety of time-resolved spectroscopic techniques allowing the dynamics to be probed at various time scales.[5−7] For example, the newest experimental advances, such as emerging X-ray free electron laser beam sources, offer unprecedented simultaneous spatial and temporal scale probes of matter.[8] Complementary computational atomistic simulations can rationalize and predict the underlying electronic and structural dynamics, being an indispensable tool for understanding fundamental physical processes and formulating material design principles. Notably, nonequilibrium dynamics in materials of interest often involves a complex manifold of intersecting and interacting electronic states. Here, the Born−Oppenheimer approximation, separating electronic and nuclear motions, breaks down, posing a conceptual challenge. Consequently, a predictive modeling framework should account for emerging nonadiabatic phenomena defining, for example, the evolution of an excitation at a level crossing such as a conical intersection.[9] These issues are commonly addressed via mixed quantum−classical (MQC) methods, such as the celebrated surface hopping (SH) approaches originating from Tully's fewest switches surface hopping (FSSH) algorithm[10] or the early mean-field Ehrenfest (EHR) approximation.[11] The MQC approaches remain computationally practical by retaining classical and quantum-mechanical descriptions for the dynamics of nuclei and electrons, respectively. However, the fundamental inconsistencies between quantum and classical mechanics and severe approximations involved generally limit the accuracy of MQC approaches. Consequently, many semiclassical and fully quantum schemes were developed entailing various levels of computational complexity and controlled approximations with respect to an exact result (we refer the reader to references in recent reviews[12−14]). Here, the commonly used methods are multiconfigurational time-dependent Hartree (MC-TDH)[15] and the related variational multiconfiguration Gaussian (vMCG) method,[16] *ab initio* multiple spawning (AIMS),[17] coupled-trajectory mixed quantum−classical method of exact factorization (CT-MQC),[16] and multiconfigurational Ehrenfest with *ab initio* multiple cloning (MCE-AIMC),[18−20] to name a few. As a result, the past couple of decades have witnessed a merging of electronic structure techniques (that provide estimates for electronic energies, wave functions, gradients of potential energy surfaces, and nonadiabatic couplings between levels) and various nonadiabatic algorithms (being essential dynamical propagators), producing versatile computational packages

Received: January 25, 2021
Accepted: March 9, 2021
Published: March 17, 2021

https://doi.org/10.1021/acs.jpclett.1c00266
J. Phys. Chem. Lett. 2021, 12, 2970−2982

permitting direct atomistic dynamics to address a broad spectrum of problems. We further refer the reader to recent comprehensive reviews[12−14,16,21,22] outlining various nonadiabatic methods and the current state of the field.

Owing to the diversity of electronic structure methods and nonadiabatic molecular dynamics algorithms, it is often difficult to evaluate the comparative performance and accuracy of different approaches in the case of realistic systems. We recall that analyzing performance for simple model cases, which permit exact numerical quantum-mechanical solutions, was an important driver for the development and improvement of MQC techniques over many years.[23] However, this luxury is lost for large and complex molecules of practical interest. Here, an interplay of various approximations involved in the electronic structure calculator/nonadiabatic dynamics driver and compromises related to the particular implementation, statistical convergences, and frequently arbitrary choice of numerical thresholds creates an obstacle that is difficult to evaluate. In this Perspective, we compare the performance of three commonly used techniques for modeling photophysics in organic conjugated materials. These methods include two MQC approaches (EHR and SH) and a fully quantum MCE-AIMC framework. By fixing our approximation for the electronic structure method at the configuration interaction singles (CIS) level and the semiempirical Austin model 1 (AM1) Hamiltonian,[24] we are able to focus on the strengths and weaknesses of these nonadiabatic dynamics approaches paying particular attention to numerical convergence across a representative set of molecules. The above simulation methods have been implemented in the nonadiabatic excited-state molecular dynamics (NEXMD) computational package.[25] Adopting a common computational framework allows us to perform direct methodological comparisons, ruling out interference from differences in implementation.

The past couple of decades have witnessed a merging of electronic structure techniques (that provide estimates for electronic energies, wave functions, gradients of potential energy surfaces, and nonadiabatic couplings between levels) and various nonadiabatic algorithms (being essential dynamical propagators), producing versatile computational packages permitting direct atomistic dynamics to address a broad spectrum of problems.

We start by briefly outlining the essence of various nonadiabatic algorithms. All three methods considered are trajectory-based methods, where an ensemble of classical Newtonian-like trajectories for the nuclei is launched from a set of initial nuclear configurations (geometries and momenta). This conformational sampling of initial conditions can be obtained from adiabatic ground-state dynamics in the presence of a thermostat (as is the case for all simulations presented here) or using other approaches, such as Wigner sampling.[26]

As an input from the electronic structure calculator, information regarding the *adiabatic* electronic states for a given configuration of nuclei, $\mathbf{R}$, is provided. This includes energies $E_a(\mathbf{R})$ (defining potential energy surfaces, PESs), adiabatic electronic wave functions $\psi_a(\mathbf{r}, \mathbf{R})$, gradients (or forces) $-\nabla_{\mathbf{R}}E_a(\mathbf{R})$, and nonadiabatic derivative coupling vectors (NACR) $\mathbf{d}_{ab}(\mathbf{R}) = \langle\psi_a(\mathbf{r}, \mathbf{R})|\nabla_{\mathbf{R}}|\psi_b(\mathbf{r}, \mathbf{R})\rangle$ parametrically depending on $\mathbf{R}$ for a manifold of electronic states labeled by indices a, b, ... (here the brackets indicate integration over the electronic degrees of freedom $\mathbf{r}$).[13]

Ehrenfest Mean Field. EHR assumes that the nuclei move classically on an effective PES, which is an average of all electronic states included in the dynamics weighted by their populations. The full time-dependent wave function for electrons and nuclei is then

$$\begin{aligned}\Psi(\mathbf{r}, \mathbf{R}, t) &= \chi_0(\mathbf{R}, t)\psi(\mathbf{r}, t)\\ &= \chi_0(\mathbf{R}, t)\sum_a c_a(t)\psi_a(\mathbf{r}, \mathbf{R}(t))\end{aligned} \tag{1}$$

where $\psi(\mathbf{r}, t)$ is a time-dependent electronic wave function at $\mathbf{R}(t)$ and $\chi_0(\mathbf{R}, t)$ is a formal normalized vibrational wavepacket. $c_a(t)$ are the state-dependent complex coefficients obtained by solving the time-dependent Schrödinger equation

$$i\hbar\frac{\partial c_a(t)}{\partial t} = E_a(\mathbf{R})c_a(t) - \frac{i\hbar}{m_{\mathbf{R}}}\sum_b \mathbf{d}_{ab}(\mathbf{R})\cdot\mathbf{P}c_b(t) \tag{2}$$

where $\mathbf{m}_{\mathbf{R}}$ and $\mathbf{P} = \dot{\mathbf{R}}\cdot\mathbf{m}_{\mathbf{R}}^{-1}$ are nuclear masses and momenta, respectively. The equations of motion for $\mathbf{R}$ and $\mathbf{P}$ obtained by the Ehrenfest Theorem are classical Hamilton's equations ($\dot{\mathbf{R}} = \mathbf{m}_{\mathbf{R}}^{-1}\cdot\mathbf{P}$ and $\dot{\mathbf{P}} = \mathbf{F}$), typically solved through Newtonian dynamics for nuclei with the force

$$\begin{aligned}\mathbf{F} = &-\sum_a |c_a(t)|^2\nabla_{\mathbf{R}}E_a(\mathbf{R})\\ &+\sum_{ab} c_a^*(t)c_b(t)\mathbf{d}_{ab}(\mathbf{R})[E_b(\mathbf{R}) - E_a(\mathbf{R})]\end{aligned} \tag{3}$$

Here, the first term is a mean-field potential across the distribution of electronic states given by the sum of gradients for all electronic states weighted according to the state populations. The second term is the "nonadiabatic" force given by the Hellman−Feynman contribution due to non-Born−Oppenheimer processes.

Notably, the classical treatment of the trajectory neglects both differences in zero-point energy for different states and tunneling. For small semirigid molecules, zero-point energy can be incorporated by sampling initial conditions through the Wigner distribution.[27] However, the Wigner distribution becomes inapplicable for large soft molecules that visit many conformational minima at room temperature, and conformers are generally sampled from classical ground-state trajectories. EHR is expected to be quite accurate for dynamic processes where PESs maintain a certain degree of coupling or when the dynamical heterogeneous evolution pathway is sufficiently homogeneous (*i.e.*, dynamics without branching). Nevertheless, it is not adequate to identify rare events during electronic relaxation, such as transient population trapping on specific electronic states or minor alternative relaxation pathways that can lead to secondary final products (*i.e.*, heterogeneous dynamics with branching). Besides, treatment of nuclear motion on the average PES becomes invalid in regions of phase space where electronic states become very

https://doi.org/10.1021/acs.jpclett.1c00266
J. Phys. Chem. Lett. 2021, 12, 2970−2982

different and are no longer coupled. It is also well-established that the EHR dynamics suffers from a continuous heating of the electronic subsystem. Thus, the longtime EHR dynamics may not recover equilibrium electronic population distributions (*i.e.*, lack of detailed balance). Finally, the neglect of electron−nuclear correlation in the Ehrenfest approach leads to improper treatment of decoherence in the electronic system. This problem was addressed in multiple studies,[28,29] and several semiempirical corrections were introduced to address the latest issues.[30,31]

Surface Hopping. The SH framework was developed to address the drawbacks of EHR. Here, the nuclei evolve on a single PES defined by a single electronic state at any given time and probabilistic stochastic hops are allowed from one electronic state to another. In the well-known *ad hoc* fewest-switches surface hopping (FSSH) method,[10] a hopping rate maintains the evolution of the electronic populations of participating states with the fewest number of hops, given by

$$P_{a\to b}(t) = \max\left[0, -\frac{\delta t \frac{2}{\hbar}\mathrm{Re}[c_a^*(t)c_b(t)[\mathbf{d}_{ab}(\mathbf{R})\cdot\dot{\mathbf{R}}]]}{c_a c_b^*}\right] \tag{4}$$

where δt is the discrete numerical time step and $c(t)$ are obtained from the EHR eq 2. An important difference compared to EHR is that the SH force for a trajectory has a single component $-\nabla_{\mathbf{R}}E_a(\mathbf{R})$ for the current PES. The hopping events are decided in a Monte Carlo-like fashion based on the switching probabilities $P_{a\to b}(t)$ evaluated between the current state a and all other states included in the dynamics. Once a hop is realized, the nuclear velocity $\dot{\mathbf{R}}$ is adjusted along the direction of $\mathbf{d}_{ab}(\mathbf{R})$ to preserve the total energy. "Frustrated" hops upward (that lack sufficient nuclear kinetic energy) are not allowed. The FSSH algorithm adheres to detailed balance and is a robust and numerically stable approach that is easy to implement. By its nature, it can identify multiple pathways (branching) associated with a given reaction or relaxation process provided a sufficient number of trajectories in the ensemble. In principle, SH requires more trajectories to achieve statistical convergence compared to EHR, and SH is not accurate for dynamic processes where PESs remain coupled all the time. Besides, it suffers from inaccuracies related to frustrated hops, energy redistribution after successful hops, and treatment of electronic coherence, among others. Also, SH approaches cannot incorporate nuclear quantum effects in a natural and straightforward manner. This triggered an enormous amount of work and appearance of modified SH algorithms that address drawbacks,[32−36] most notably introducing decoherence corrections.[13,21,29,33,37−39]

Multiconfigurational Ehrenfest with *Ab Initio* Multiple Cloning. MCE-AIMC is a fully quantum approach and a controlled approximation beyond MQC methods that combines two developments, namely, the MCE dynamics approach and the AIMC correction, the latter being a basis sampling technique. Let us first consider the MCE approach. MCE is a generalization of the EHR approach that makes use of ensembles of individual EHR trajectories considered as trajectory-guided Gaussian basis functions (TBFs) $\Psi^{(n)}(\mathbf{r}, \mathbf{R}, t)$. The full quantum wave function of electrons and nuclei is then represented as

$$\begin{aligned}\Psi(\mathbf{r}, \mathbf{R}, t) &= \sum_n d^{(n)}(t)\Psi^{(n)}(\mathbf{r}, \mathbf{R}, t) \\ &= \sum_n d^{(n)}(t)\chi^{(n)}(\mathbf{R}, t)\sum_a c_a^{(n)}(t)\psi_a(\mathbf{r}, \mathbf{R}_n(t))\end{aligned} \tag{5}$$

where the index n denotes the nth Ehrenfest configuration with $\Psi^{(n)}(\mathbf{r}, \mathbf{R}, t)$ and $c_a^{(n)}(t)$ is the electronic wave function coefficient from eq 2 (compare eq 5 to eq 1). The nuclear wave functions $\chi^{(n)}(\mathbf{R}, t)$ or $|\chi_n\rangle$ are given by coherent states,[40,41] which, in the coordinate representation, are Gaussian functions centered in EHR trajectories with coordinates $\mathbf{R}_n$ and momenta $\mathbf{P}_n$:

$$\begin{aligned}\chi^{(n)}(\mathbf{R}, t) = \left(\frac{2\boldsymbol{\alpha}}{\pi}\right)^{N_{\mathrm{dof}}/4} \exp\Big(&-\boldsymbol{\alpha}(\mathbf{R} - \mathbf{R}_n(t))^2 \\ &+ \frac{\mathrm{i}}{\hbar}\mathbf{P}_n(t)(\mathbf{R} - \mathbf{R}_n(t)) + \frac{\mathrm{i}}{\hbar}\gamma_n(t)\Big)\end{aligned} \tag{6}$$

Here, N_{dof} is the number of nuclear degrees of freedom of the system. The diagonal Gaussian variance matrix $\boldsymbol{\alpha}$ contains width parameter values α that depend on the atomic species, and $\gamma_n(t)$ is a phase. $\psi_a(\mathbf{r}, \mathbf{R}_n)$ are electronic eigenstates at the center of the wave packet $\mathbf{R}_n$. This basis of electronic wave functions that is custom for each TBF and changes with its motion has been termed the time-dependent diabatic basis set (TDDB)[19] (note that this term is distinguished from the standard time-independent diabatic basis notion). The time-dependence of the electronic states $\psi_a(\mathbf{r}, \mathbf{R}_n(t))$ due to the motion $\mathbf{R}_n(t)$ leads to nonadiabatic coupling in the TDDB formulation of MCE. Notice that the majority of nonadiabatic dynamics theories, including the original formulation of AIMC, use the basis of adiabatic states $\psi_a(\mathbf{r}, \mathbf{R})$, which assume their dependence on nuclear coordinates $\mathbf{R}$. In all such theories, nonadiabatic coupling arises from the kinetic energy operator acting on $\mathbf{R}$-dependent electronic functions. However, the basis $\psi_a(\mathbf{r}, \mathbf{R})$ fails when adiabatic states change abruptly, which often happens in large molecules, for example, at so-called trivial unavoided crossings. In the adiabatic formulation, kinetic energy operators yield nonadiabatic coupling terms that include both first and second derivatives of the wave function, and the second-order term is then neglected; however, the validity of such an approximation is sometimes questioned. In TDDB, where nonadiabatic coupling arises from the time dependence of the electronic basis functions, the second derivative term does not appear and no approximation related to it is needed. Among other advantages of using the wave functions $\psi_a(\mathbf{r}, \mathbf{R}_n)$ is that this approach naturally accounts for the geometric phase effect.[42]

In the MCE approach, the motion of the centers of Gaussians $\mathbf{R}_n$ and $\mathbf{P}_n$ and the evolution of the amplitudes $c_a^{(n)}$ is determined by the same set of equations (eqs 1−3) as in the EHR approach, and the phase evolves as $\dot{\gamma}_n = \mathbf{P}_n\cdot\dot{\mathbf{R}}_n/2$. Thus, the parameters describing the TBF evolution are solved using classical equations of motion first prescribed by Heller.[43] For practical considerations, however, the width, α, is taken as a "frozen" free-parameter. Solving for the width parameter, as suggested by Heller, is simply too expensive for large molecular systems as it requires the full Hessian to be calculated on-the-fly for each configuration. This parameter is potentially critical to the quality of the basis. However, a reasonable choice for α, paired with a sufficient number of basis functions, should lead to a reasonable basis and a small dependence on the parameter

https://doi.org/10.1021/acs.jpclett.1c00266
J. Phys. Chem. Lett. 2021, 12, 2970−2982

for model systems. The basis, in general, is far from complete for real molecules. Finally, the additional configurational coefficient, $d^{(n)}(t)$, is obtained using the time-dependent Schrödinger equation

$$\sum_n \langle \Psi^{(m)}(t)|\Psi^{(n)}(t)\rangle \dot{d}^{(n)}(t) = -\frac{\mathrm{i}}{\hbar}\sum_n \left(H_{mn} - \mathrm{i}\hbar\langle \Psi^{(m)}(t)|\frac{\mathrm{d}}{\mathrm{d}t}|\Psi^{(n)}(t)\rangle\right) d^{(n)}(t) \quad (7)$$

where $H_{mn} = \langle \Psi^{(m)}|\hat{H}|\Psi^{(n)}\rangle$ are matrix elements of the Hamiltonian. In principle, this makes MCE a formally exact fully quantum method, free of approximations made in EHR or SH theories, as the trajectories here determine only the evolution of the basis set $\Psi^{(n)}(\mathbf{r}, \mathbf{R}, t)$, while time-evolution of the wave function itself is given by eq 7. In practice, approximations in the basis sampling and solution of the Hamiltonian matrix elements are made.[44] More details and technical implementations of the MCE method can be found elsewhere.[18,20,27]

To ensure convergence, the ensemble of EHR trajectories or TBFs must span all relevant regions of configurational space. That is, the functions $\Psi^{(n)}$ should ideally form a complete basis representing the exact $\Psi(\mathbf{r}, \mathbf{R}, t)$ for the entire dynamics considered. The finite size of the basis $\Psi^{(n)}$ is a major approximation of MCE. In order to improve the basis, different sampling techniques have been proposed[18] and tested.[40] In particular, the AIMC approach overcomes the problem of the EHR mean-field dynamics by avoiding unphysical electronic and nuclear configurations which do not form a good basis for $\Psi(\mathbf{r}, \mathbf{R}, t)$. Namely, each Ehrenfest trajectory is allowed to clone into two copies upon level crossing if the PESs of crossing states are sufficiently different. While there is no strict prescription for cloning events, different AIMC cases have been quantified by defining three numerical cloning criteria used in our previous work,[18] followed by an alternative set of criteria for implementation in the NEXMD.[20] Briefly, the first cloning criterion identifies situations in which at least two adiabatic electronic states are sufficiently populated. The second criterion analyzes whether the average EHR force is no longer representative of individual state contributions, indicating a breakdown of the mean-field approximation of the EHR trajectory. That is, the extent to which the state-specific force contribution from the most populated excited state matches the direction of the mean-field driving force. Finally, the third criterion limits the cloning events to regions of phase space where the electronic states are not strongly coupled. All three cloning criteria are evaluated with respect to a set threshold (see Methods). Each time the set of cloning criteria is fulfilled, the AIMC algorithm replaces the original EHR trajectory with two new trajectories and does not change the wave function. Both configurations then evolve independently, making an efficient augmentation of the set of TBFs. This restores correlation between electronic states and nuclear motion. While this procedure has the benefit of naturally accounting for decoherence events and bifurcating relaxation pathways, it comes at the expense of rapidly increasing computational cost. In particular, trajectories are not annihilated in this formulation. Therefore, it must be restricted to situations in which it represents a significant contribution to the final accuracy of the results, accomplished by imposing threshold values on the cloning criteria.

The use of "trains" is another helpful sampling trick used by MCE-AIMC. Trains consist of a number of basis functions that follow each other along the same trajectory with some time delay. This allows electronic structure data, which is the most expensive part of direct dynamics, to be reused. Finally, MCE-AIMC uses the so-called bra-ket expansion for evaluation of the coupling between Ehrenfest configurations, which requires only electronic structure data that has already been obtained while running the trajectories.[18] This conveniently allows efficient parallel propagation of the independent trajectory ensemble followed by a simple post processing of the data. The accuracy of this approximation has been verified.[44] More advanced MCE functions are currently under development to perform on-the-fly MCE-AIMC simulations to accommodate large molecular systems and long running times. The above sampling approaches greatly improve the accuracy and convergence of the MCE-AIMC technique.

Generally, out of the three methods (EHR, SH, and MCE-AIMC), the EHR method converges the fastest; however, the nonadiabatic contribution to the force (eq 3), which is not present in the SH force, requires calculation of the NACR vector at every step and shorter dynamical time steps because of its spiky behavior. Subsequently, EHR and SH carry approximately similar numerical cost (depending on a particular implementation). The MCE-AIMC approach is about 5−10 times more expensive compared to EHR, depending on the selection of the sampling techniques, cloning thresholds, and/or the frequency of cloning events, calling for comparative studies of the accuracy and convergence of results for optimal performance. Finally, we mention the difference between MCE-AIMC and the *ab initio* multiple spawning (AIMS) approach developed by the Martínez group.[17,45] Both approaches are similar in spirit except that AIMC is based on EHR trajectories and represents a natural way of bifurcating the wave function without the complications of spawning algorithms.

Because of their simplicity and reasonable numerical cost, both EHR and SH have been broadly used for modeling of nonadiabatic dynamics. Despite different advantages and disadvantages, compared to EHR, SH approaches have gained more popularity. For example, SH methods were routinely used to study the photophysics and photochemistry of a variety of systems including organic chromophores (*e.g.*, dendrimers, polymers, metal−organic complexes, graphene, *etc.*), biosystems (*e.g.*, chlorophylls, retinal, and nucleotides), and semiconductor nanostructures (*e.g.*, quantum dots, 2D materials, and perovskites).[22,46−51] Among the different computational packages that make use of SH implementations to perform hybrid quantum/classical direct dynamics simulations, we can mention NEWTON-X,[52] SHARC (Surface Hopping including Arbitrary Couplings),[53] PYXAID (Python eXtension for *Ab Initio* Dynamics),[54] and NEXMD (Nonadiabatic EXcited-states Molecular Dynamics),[25] among others. The situation is different for numerically demanding and accurate MCE-AIMC

Because of their simplicity and reasonable numerical cost, both EHR and SH have been broadly used for modeling of nonadiabatic dynamics.

https://doi.org/10.1021/acs.jpclett.1c00266
J. Phys. Chem. Lett. 2021, 12, 2970−2982

and AIMS where only a few implementations are available,[14,20] and applications were limited to systems generally smaller than those that were treated with EHR and SH techniques.

NEXMD Implementation. All three methods described above have been implemented in the NEXMD software package[25] that has been developed to perform direct nonadiabatic molecular dynamics simulations of photoinduced processes across a variety of time scale up to tens of picoseconds. The NEXMD targets large multichromophoric molecules involving a manifold of coupled electronic excited states. The numerical cost of simulations is reduced by using a family of semiempirical Hamiltonians[55] as well as a minimalistic description of excited states at the configuration interaction singles (CIS) or time-dependent Hartree−Fock (TDHF) levels. Subsequently, excited-state energies, gradients, and nonadiabatic couplings are calculated *on-the-fly* using the collective electronic oscillator (CEO) approach.[13,25,56] All NEXMD simulations typically involve the propagation of a swarm of classical trajectories, where the initial conditions are sampled via constant-temperature ground-state molecular dynamics trajectories computed in the presence of a thermostat (*e.g.*, Langevin thermostat[57]). Such sampling addresses the complex conformations that soft molecular structures can adopt at given conditions, whereas stochasticity and branching of individual trajectories enter through the specificity of nonadiabatic algorithms, as described above. Another important feature for all simulations is proper identification and correction for trivial unavoided crossings which appear as a consequence of adapting the adiabatic (vs diabatic) electronic basis for dynamical trajectories. Specifically, trivial unavoided crossings are defined as intersections of two noninteracting adiabatic states evidenced by a sharp, strongly time-localized peak in the nonadiabatic couplings of the respective adiabatic state wave functions occurring only at the exact energy degeneracy and becoming vanishingly small elsewhere. Treatment of trivial unavoided crossings can be achieved by following the diabatic passage in direct dynamical simulations.[35] More details concerning the NEXMD workflow and parameters can be found elsewhere,[25,56] particularly, for SH,[25,56] EHR,[13,20] and MCE-AIMC[19,20] implementations. The specific NEXMD simulation details, parameters, and AIMC cloning procedures used here are provided in Methods. Meanwhile, all three methods (EHR, SH, and MCE-AIMC) are also implemented in the linear-response time-dependent density functional theory-based computational package NWChem[58,59] to provide more accurate calculation at the full *ab initio* level.

Studied Molecules. To evaluate the performance of SH, EHR, and AIMC methods (throughout the remaining sections, AIMC refers to the MCE-AIMC approach), we consider a set of realistic molecular systems relevant to energy-harvesting applications. Beyond exploring effects of different sizes and concomitant increase of excited-state density, we also consider characteristic excited-state structures. It is also important to realize the effect of gradually increasing the possibility of wave function bifurcations and resulting effects on coherent electronic−vibrational dynamics[60] on the accurate description of the photoinduced relaxation. We base our selection on dendritic systems, which are multichromophore chemically bound molecular systems with highly branched structures that present exceptional light-harvesting capabilities[61] over a broad region of the solar spectrum. The efficiency of the energy transfer between the different chromophore units is conditioned by their particular spatial assembly. Notably, dendrimers composed of poly(phenylene ethynylene) (PPE) building blocks have been the subject of several theoretical and experimental studies.[62−65] Photoexcited PPE dendrimers experience an ultrafast energy transfer involving multiple possible pathways in which through-bond and through-space mechanisms can take place among different chromophore units within the highly branched structures.[64,66−68] Their inherent intramolecular energy redistribution depends on how the multiple units are assembled, affecting their spatial distances and relative orientations. Every linear segment of PPE is associated with one or more excited states typically localized on this segment in the static case for ground-state optimal geometry. The dendrimer backbone configuration then impacts the relative strength of couplings between chromophore units and the balance between the different energy transfer mechanisms.[69]

In the present Perspective, we simulate the photoinduced nonadiabatic molecular dynamics of different combinations of PPE dendrimer building blocks, namely, 2PPE, 22PPE, 222PPE, 233PPE, and 2233PPE (shown as insets in Figure 1), where numbers indicate the lengths of PPE chromophore units. We set our simulations (see Methods for specific

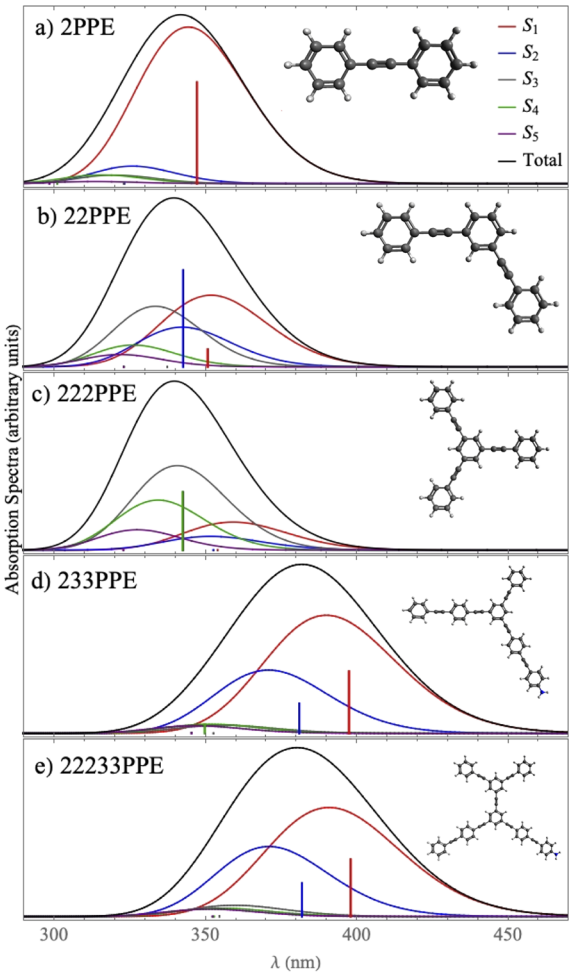

Figure 1. Absorption spectra for (a) 2PPE, (b) 22PPE, (c) 222PPE, (d) 233PEE, and (e) 2233PPE showing contributions from the lowest-energy adiabatic excited states to the total spectrum. Sketches of the molecules are shown as insets. Vertical lines indicate oscillator strengths of excited states calculated at the ground-state minimum.

https://doi.org/10.1021/acs.jpclett.1c00266
J. Phys. Chem. Lett. 2021, 12, 2970−2982

parameters and simulation setups) to mimic typical experimental time-resolved spectroscopic probes performed on solution samples at ambient conditions.[64,65,70,71] Here, initial photoexcitations for a set of conformational samples are created by populating higher-energy optically allowed excited states within a chosen experimentally relevant spectral window. Subsequently, an ensemble of excited-state trajectories is propagated on an ultrafast time scale duration of a few hundred femtoseconds using different algorithms for nonadiabatic dynamics. Importantly, the same electronic structure model chemistry (AM1/CIS) is used for all calculations (see Methods). Typically, most of the trajectories end on the lowest S_1 state because of efficient nonradiative relaxation concomitant to energy transfer processes. The relaxation time scales and dynamics of the trajectory ensembles for SH, EHR, or AIMC approaches are then compared and analyzed.

Structure of Excited States and Absorption Spectra. We start our analysis with the absorption spectra for the PPE dendrimer systems shown in Figure 1. The spectra were calculated according to the procedure outlined in Methods. The main contributing peaks defined by the individual excited states to the total spectrum change among the different molecular systems. Importantly, a significant overlap between these characteristic features is observed for all systems. This is mainly attributed to dynamical dihedral rotations between phenylene units, mixing the lowest excited states and introducing structural distortions that change their spatial localization (Figure S1).[72,73] Comparison of absorption lineshapes obtained from dynamics with "static" calculation of excited states and their oscillator strengths at the global geometry minimum, shown as vertical sticks in Figure 1, provides an important initial analysis of excited-state structure across the considered molecular family. Generally, each linear conjugated PPE segment contributes a single strong absorption peak associated with its lowest "band gap" S_1 transition owing to the excitonic nature of $\pi-\pi^*$ electronic transitions (Figure 1a, red stick). Thermal fluctuations at ambient conditions ensure minor contributions of higher-energy states to the absorption (Figure 1a, individual state absorptions). Meta-linked linear segments of the same length form a molecular dimer with two contributing excited states (Figure 1b, sticks), which can be readily rationalized by invoking the concept of a Frenkel exciton system[74] where the states of a multimer present a coherent superposition of monomeric states interacting via electrostatic coupling (the point-dipole approximation is frequently invoked for calculations of these couplings in the case of Förster resonant energy transfer systems). Importantly, this ideal picture breaks because of thermal fluctuations that involve several states in the dynamics (Figure 1b, individual state absorptions and Figure S1 for orbital plots of excited-state transition densities), necessitating atomistic nonadiabatic simulations beyond simple models. A similar picture holds in the case of the trimer (Figure 1c), where the ideal model gives a doubly degenerate pair of lowest states and an optically forbidden next one. As expected, conformational dynamics breaks the symmetry and involves contributions from five states. A similar consideration can be applied for the remaining two largest molecular choices (Figure 1d,e). Here longer linear segments lead to red shifts of essential excited states. Thus, two three-unit linear segments contribute a pair of lowest-energy essential excited states for both molecules. Shorter two-unit segments add one state per segment, respectively, for systems in Figure 1d,e. As seen above, this idealized picture gets invalidated by thermal fluctuations.

We begin our nonadiabatic molecular dynamics simulations by initially exciting the 370 nm spectral region corresponding to state S_3 for all molecular systems except for 233PPE in which state S_5 was initially excited. We further compare the dynamics of nonradiative relaxation toward the lowest-energy S_1 state in all molecular systems for the three simulation methods in question.

Comparison of Method Performance. The electronic energy relaxation process after photoexcitation can be monitored by the evolution of the adiabatic electronic state populations. In EHR and AIMC simulations, state populations are expressed as *quantum populations*, defined as the quantum probability for the state obtained as the square of the quantum coefficients averaged over the ensemble of trajectories (eq 2). In SH simulations, state populations can be expressed as either quantum populations or as so-called *classical populations*, with the latter defined as the fraction of trajectories evolving on the state of interest at any given time. Internal inconsistency due to lack of decoherence corrections in SH is frequently manifested as a discrepancy between classical and quantum populations. The implementation of some form of decoherence corrections into SH-like algorithms have been shown to overcome this deficiency.[13,21,38] For example, the *ad hoc* instantaneous decoherence introduced in our SH simulations[38] leads to depletion of the quantum amplitudes in high-energy states and closely synchronizes evolution of classical and quantum populations. Thus, we follow evolution of classical populations in SH only.

Figure 2 shows the comparison of EHR state populations and SH classical populations. In all systems, the SH method leads to faster relaxation times than EHR. The presence of forbidden hops in SH generally prevents expected population transfer to higher-energy states. For example, this partially hinders the $S_1 \rightarrow S_2$ population transfer illustrating another frequently discussed aspect of SH methods. For 22PPE, 222PPE, and 2233PPE systems, EHR simulations display oscillatory interchange of electronic populations, which are only weakly observed in SH populations. Notably, this trend persists even in the absence of SH decoherence correction, as shown in Figure 3 and discussed later. This reflects previously reported electron-vibrational coherent dynamics[75] associated with electronic excited states spatially localized in equivalent chromophore units,[76] as is the case for systems with more than one 2-ring chromophore unit. EHR simulations lead to an intrinsically more coherent behavior of electronic populations than SH, even though both methods have been previously described as "overcoherent" because they lack electronic decoherence mechanisms. We note that electron-vibrational coherent dynamics includes phase-correlated electronic and vibrational motions across the entire trajectory ensemble. The EHR trajectories result in such strong correlations owing to their mean-field nature lacking dephasing of vibrational wavepackets on different PESs. In contrast, stochastic and completely classical adiabatic trajectories in SH dephase rapidly in the ensemble. Thus, these methods represent limiting cases and neither of them is quantitative for describing electron-vibrational coherence because neither SH nor EHR explicitly incorporates evolution of vibronic wavepackets. Notably, the appearance of coherent oscillations in EHR is distinctly different across the family of molecular systems considered. For example, 2PPE with well-separated excited

https://doi.org/10.1021/acs.jpclett.1c00266
J. Phys. Chem. Lett. 2021, 12, 2970−2982

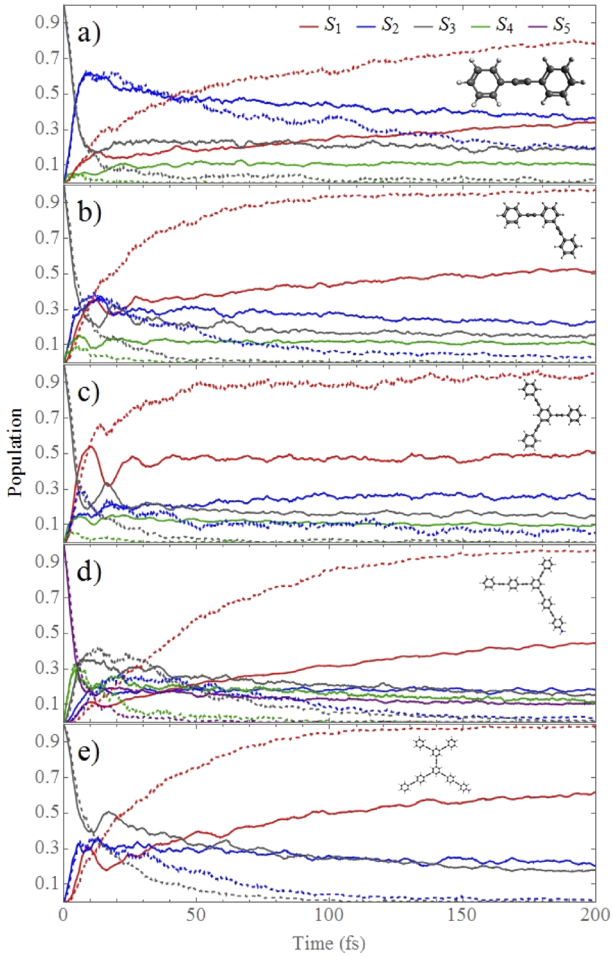

Figure 2. Time evolution of the adiabatic electronic state populations averaged over 300 SH trajectories using decoherence correction (dashed lines) and 300 EHR trajectories (solid lines). Here SH populations are expressed as classical populations.

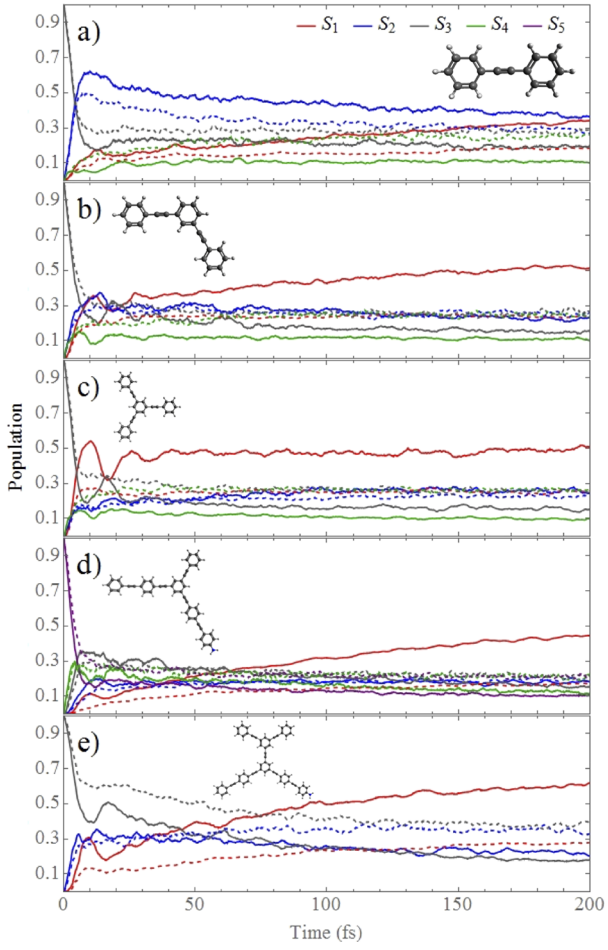

Figure 3. Time evolution of the adiabatic electronic state populations averaged over 300 SH trajectories without using decoherence correction (dashed lines) and 300 EHR trajectories (solid lines). Here SH populations are expressed as quantum populations.

states of different nature essentially lacks this phenomenon. In contrast, these oscillations are clearly present in 22PPE and 222PPE cases, which feature electronically coupled manifold Frenkel-exciton states as discussed above. As mentioned, the EHR method is expected to be more accurate for dynamical processes where the coupling between states persists in time. This is the case for the earlier times of our simulations during which the molecular system evolves in regions of phase space close to the conical intersection seam. At longer times, however, nuclear motion on the average PES between the S_1 and S_2 states persists in the EHR, even after these states are no longer coupled. This appears to slow the relaxation process.

In order to further analyze differences between SH and EHR, we compare behavior of EHR and SH quantum populations (the latter are obtained without applying *ad hoc* decoherence corrections) as shown in Figure 3. Here SH quantum populations show very slow relaxation to the S_1 state during the simulation time compared to the EHR results. Additionally, as was observed previously, the coherences are well-pronounced in EHR compared to the SH case across the board. Even though the quantum populations in both approaches are calculated with eq 2, the main difference between the evolution of the EHR and SH electronic wave function arises from the propagation of nuclei according to the average EHR force compared to a state-specific SH force at each time. The average EHR force (eq 3) is composed of a population weighted force (first term in eq 3) and a nonadiabatic contribution (second term in eq 3). It is the nonadiabatic force that is responsible for enhancing vibrationally induced electronic population exchange and faster population relaxation. While this nonadiabatic Hellman−Feynman force is explicitly included in EHR simulations, it appears only indirectly in SH through the *ad hoc* adjustment of velocities in the direction of the nonadiabatic coupling vector after a hop. Therefore, compared to the explicit treatment in EHR, the random nature of this force in SH seems to be the reason for the lack of quantum beating in SH quantum populations. Previous works have shown that EHR simulations are able to better reproduce experimentally observed coherent oscillations between electronic states where SH fails.[77]

Thus, while the SH and EHR results are consistent in describing nonradiative relaxation in all molecules, they are qualitatively different across several features. In order to discern between these methodologies, we next benchmark these results against a more accurate AIMC method that naturally incorporates electronic decoherence. Figure 4 shows the comparison between EHR and AIMC simulations. AIMC simulations present faster relaxation than EHR but are slower than SH simulations. Notably, by construction, AIMC trajectories explore larger areas of configurational space than

https://doi.org/10.1021/acs.jpclett.1c00266
J. Phys. Chem. Lett. 2021, 12, 2970−2982

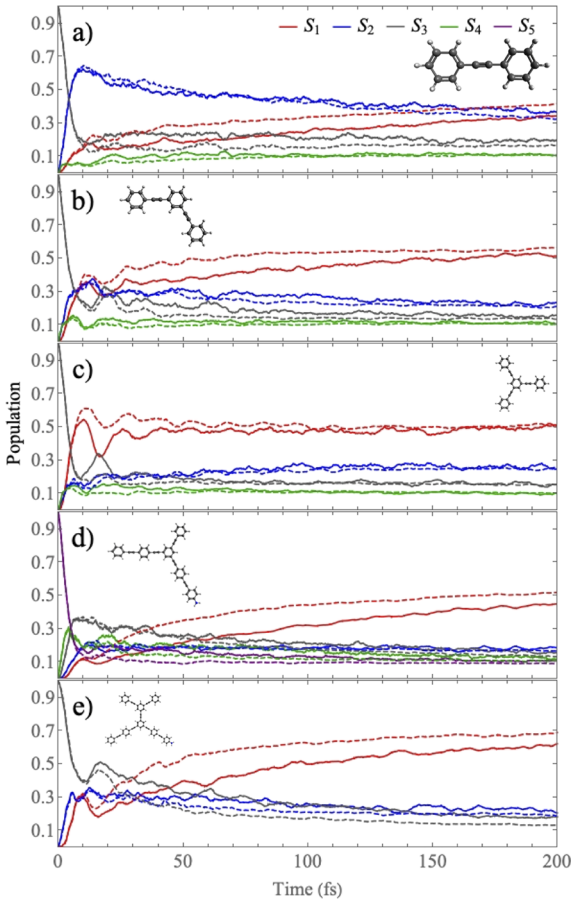

Figure 4. Time evolution of the adiabatic electronic state populations averaged over 300 AIMC trajectories (dashed lines) and 300 EHR trajectories (solid lines).

EHR simulations. Cloning events incorporate the sampling of regions of phase space dominated by relaxation pathways involving state-specific vibrational fluxes which are not explored by EHR simulations. Moreover, AIMC results are free from artifacts imposed by mean-field dynamics, as described above. In this sense, AIMC manages to capture aspects of the nuclear dynamics covered by SH simulations, particularly once S_1 and S_2 states are no longer coupled. As has been discussed previously, for SH simulations, these relaxation pathways dominated by state-specific vibrations lead to a Shishiodoshi-like unidirectional energy transfer.[66] That is, once the electronic population has been transferred to S_1, SH trajectories follow different pathways on either the S_1 or S_2 PES. Trajectories reaching the S_1 state steer in phase space to regions of low nonadiabatic coupling, while trajectories remaining on S_2 remain in regions of strong nonadiabatic coupling, which facilitates subsequent fast relaxation to S_1. This behavior consistently emerging in SH simulations is also reproduced by the cloning events in AIMC simulations. This is particularly relevant for 233PPE and 2233PPE systems (Figure 4d,e) that experience effective 2-ring → 3-ring unidirectional energy transfer. It is also important to note that as AIMC naturally incorporates decoherence, it exhibits damped quantum beating compared to EHR that lacks decoherence mechanisms.

AIMC Convergence and Parameters. The accuracy of AIMC relies on its convergence and robustness with respect to different parameters that should be tested and compared: the number of trajectories, the number of allowed cloning events per initial condition, and changes in the Gaussian width parameter α (eq 6). Our AIMC results that track the S_1 state population growth are presented in Figure 5, and all of the relevant parameter variations are summarized in Table S1. The corresponding error plots for data shown in Figure 5 are provided in Figure S2, where the error is calculated as a relative difference with respect to our most accurate AIMC result.

First, we analyzed the convergence of the electronic relaxation with respect to the number of trajectories using 600 trajectories as our reference for comparison. The AIMC

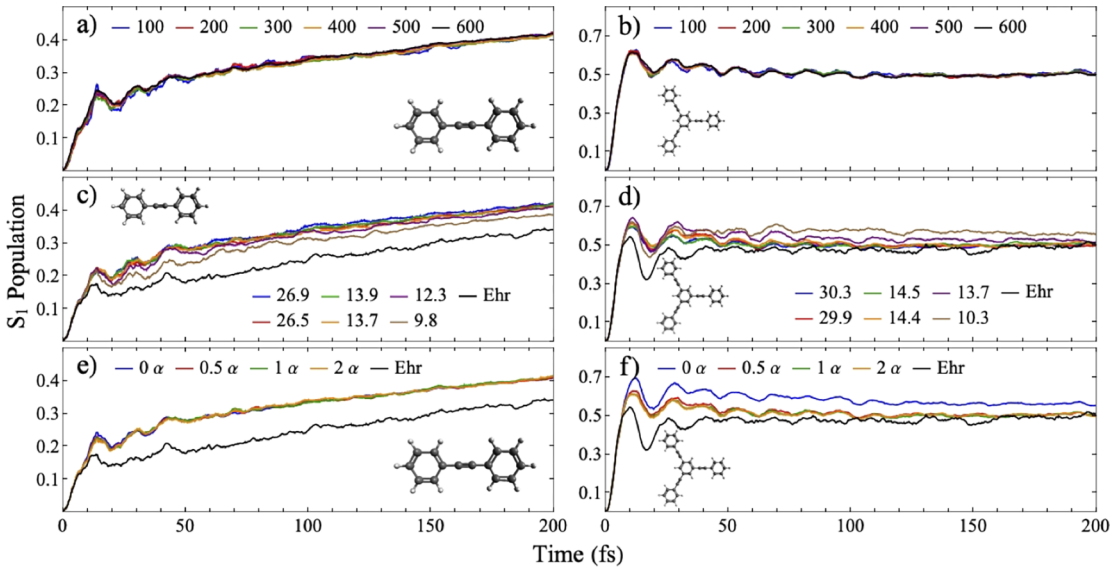

Figure 5. Comparison of the time evolution of the average population on the S_1 adiabatic state obtained from EHR and AIMC simulations using different parameters. (a and b) Convergence of AIMC results with respect to the number of trajectories for 2PPE and 222PPE, respectively. (c and d) Convergence of AIMC results with respect to the number of cloning events per initial condition for 2PPE and 222PPE, respectively. (e and f) Analysis of robustness of AIMC results with respect to variations in the α [Bohr^{-2}] Gaussian width for 2PPE and 222PPE, respectively.

https://doi.org/10.1021/acs.jpclett.1c00266
J. Phys. Chem. Lett. 2021, 12, 2970−2982

simulation results using ensembles varying from 100 to 600 trajectories are shown in panels a and b of Figure 5 for the 2PPE and 222PPE systems, respectively. AIMC convergence is achieved qualitatively using only 100 trajectories; however, errors (Figure S2) of up to 5% persist beyond 50 fs for both systems. Using 200 initial trajectories substantially reduces these spikes in error and reproduces the results obtained with 600 initial trajectories within 1% on average.

Next, we investigate the convergence of AIMC results with respect to the number of allowed cloning events per initial condition. For this purpose, we gradually relax the cloning threshold in order to accept more cloning events per trajectory (see Table S1 for exact parameters). The MCE/EHR result corresponds to a limiting case of no cloning events. The highest obtained number of cloning events serves as our reference for comparison. Figure 5c,d shows that no significant improvement is observed once an average of ∼13 cloning events per initial trajectory is reached for both 2PPE and 222PPE systems. Errors less than 5% (Figure S2) are achieved for relatively few cloning events. This effect is mainly due to a fast drop in statistical weight (due to low population) of a cloned trajectory after each bifurcation. Up to now, we have seen that the bifurcations of the wave function in AIMC allow the system to find faster relaxation pathways. That is, the S_1 populations for AIMC grow faster compared to the EHR results, and increasing the number of cloning events further increases relaxation (as in Figure 5c). This dependence may be weak and nontrivial as in the case of 222PPE seen in Figure 5d. The coherent oscillations follow an opposite trend and generally reduce with an increase of bifurcations. Thus, starting from 200 initial trajectories and allowing up to ∼10 cloning events per trajectory lead to a reasonably numerically accurate AIMC description, at least for the molecular systems considered here.

Finally, we examined the dependence of AIMC results with respect to variations in the Gaussian width parameter α (eq 6). Here, we vary the Gaussian width from 0α to 2α, and results are evaluated in comparison to the optimal value 1α (4.7 Bohr^{-2} for hydrogen and 22.7 Bohr^{-2} for carbon) according to Thompson *et al.*[78] Figure 5e,f indicates that AIMC results weakly depend on α, unless it is set to zero. Cloning events have two effects: one is related to the population exchange between trajectories, and the other restricts the unphysical mean field exploration of phase space by Ehrenfest trajectories. Setting α to zero eliminates the overlap between configurations and thus neglects any population transfer between trajectories, and therefore, any nuclear quantum effects are also neglected. This leaves only the correction related to the rectification of the mean field. When α is set to zero, the result is unaffected for 2PPE but substantially differs for 222PPE. For 2PPE, there are no quantum effects, whereas for 222PPE vibronic coherences are present as evidenced by the oscillatory S_1 populations discussed above. Therefore, the transfer of population between configurations is important in 222PPE, resulting in 10−15% error when neglected (Figure S2). The otherwise independent AIMC result with respect to the value of α is expected for complex molecular systems with hundreds of nuclear degrees of freedom subjected to thermal structural distortions at room temperature. The overlap between nuclear wave functions of cloned trajectories drops very fast after bifurcation, and details about the magnitude of each individual overlap are washed out in the average over all nuclear degrees of freedom. To this end, our tests show relative stability of the results with respect to the Gaussian width α, and therefore usage of standard parameters fitted by Thompson *et al.*[78] is advised.

In conclusion, modeling of nonadiabatic excited-state dynamics on the atomistic scale in molecular and solid materials has gradually become a mainstream task of computational chemistry with a variety of algorithms available through several computational packages. Generally, these simulations are much more numerically expensive compared to typical Born−Oppenheimer *ab initio* molecular dynamics in the ground or excited state. A practitioner is faced with the problem of choosing an appropriate combination of a nonadiabatic algorithm and model chemistry for electronic structure that provides an optimal numerical price/accuracy ratio. Moreover, an adequate conformational sampling of "soft" molecular systems at room (or even low) temperature is a key component for numerical simulations mimicking experimental conditions. As such, reported results are frequently subjected to a particular implementation of a nonadiabatic algorithm, convergence of statistical averages for trajectory ensembles, and numerical thresholds. Here, a comparative analysis can identify strengths and flaws in approximate and *ad hoc* approaches, ultimately allowing for reduced numerical expenses and providing guidelines for selecting an optimal setup for specific numerical simulations of a target system. Unfortunately, only a few studies have been done to compare performance of different methods, particularly, targeting large systems. Typically, comparisons for SH and EHR have been performed using small molecules or low-dimensional model systems.[29,79,80] Comparisons of SH and EHR are also common in development of new variations of SH or EHR-like methods.[29,30,39,81]

In this Perspective we compare the performance of three common nonadiabatic algorithms (SH, EHR, and AIMC) broadly used for modeling of nonradiative relaxation of exited states. We select a sufficiently diverse set of molecular systems (dendritic segments of different size) reflecting typical cases of molecular chromophores and model excited-state dynamics relevant to typical experimental time-resolved spectroscopic probes. Distinguishing population relaxation and coherent electron-vibrational dynamics over a large equilibrated sampling provides insight into the heterogeneity of photo-excited pathways taking place in different regions of the conformational space. Overall, the rate of nonradiative transitions defining population relaxation is fastest in the SH algorithm, whereas the EHR approach provides slower rates. The more accurate AIMC technique generally provides values in between. Coherent electron-vibrational dynamics over heterogeneous ensembles of trajectories is most pronounced in EHR and to a lesser extent in SH. The AIMC technique, featuring natural decoherence using trajectory cloning to account for wave function bifurcations, indicates persistence of electron-vibrational phenomenon on a time scale of a few hundred femtoseconds in between the EHR and SH results.

Altogether, we have been able to quantitatively evaluate EHR, SH, and AIMC methods for the first time by using the common theoretical framework provided by the NEXMD software package and the same molecular systems. Despite quantitative differences, we have found that EHR and SH provide qualitatively equivalent descriptions of nonadiabatic processes, while AIMC provides an adequate and feasible method that corrects the EHR weakness associated with quantum coherences and unphysical mean field nuclear

https://doi.org/10.1021/acs.jpclett.1c00266
J. Phys. Chem. Lett. 2021, 12, 2970−2982

Our results suggest that efforts aimed at improving AIMC offer a viable route to increasing the accuracy of nonadiabatic dynamics simulations as an alternative to further *ad hoc* improvement of the EHR and SH methods.

motions. This result suggests that efforts aimed at improving AIMC offer a viable route to increasing the accuracy of nonadiabatic dynamics simulations as an alternative to further *ad hoc* improvement of the EHR and SH methods. We suggest AIMC as a method whose future improvements can lead to proper treatment of nuclear quantum effects not properly explored in commonly used approaches, such as tunneling, zero point energy, and wave packet spreading, and better complement experiments, such as coherent control and time-resolved multidimensional spectroscopies. Moreover, the fast convergence of AIMC results with respect to that for SH and its robustness with respect to different parameters seem to guarantee its stability under new improvements (*e.g.*, nuclear quantum effects and coupled trajectories) and the reduced computational costs that these future explorations could cause. The obtained insights have shed light on the advantages and disadvantages of the different methods considered. We hope this work contributes to the development of new improvements and provides practical guidelines for both modelers and spectroscopists aiming to apply nonadiabatic excited-state dynamics simulations for investigating internal conversion or carrier transport dynamics in extended molecular systems

METHODS

In order to carry out direct comparisons, simulations using different methods were performed with as uniform a set of parameters as possible. Unless otherwise noted, the same parameters are used for each molecular system. Adiabatic ground-state dynamics for conformational sampling of initial conditions was performed using Langevin dynamics to maintain an equilibrated temperature of 300 K with a friction coefficient of 20 ps^{-1}. A time step of 0.5 fs was used to generate a 1 ns ground-state trajectory. The absorption spectra in Figure 1 were then obtained by collecting vertical transition energies and oscillator strengths calculated from 1000 equilibrated ground-state conformational samples. The contribution from each excited state is modeled using a Gaussian line shape according to ref 25 with a broadening of 0.1 eV. The total spectrum is the average of the contributions from all configurations. Next, 300 ground-state geometries and momenta were sampled to form the ensemble of excited-state trajectories. The nonadiabatic trajectories were initialized from S_3 (S_5 for 233PPE) where 4 lowest-energy excited states were included in the dynamics (5 states for 233PPE; 3 states for 2233PPE) (see Figure S1). Nonadiabatic trajectories were propagated using constant energy dynamics for 200 fs with a time step of 0.1 fs for SH and 0.05 fs for EHR and AIMC simulations. For all methods, trivial unavoided crossings were detected following ref 35 by reducing the time step by a factor of 40. Following our previous work analyzing the sensitivity of SH results to the type of decoherence correction,[38] the SH simulations utilize the instantaneous decoherence correction (unless otherwise noted) where quantum coefficients are reinitialized following all attempted hops, including frustrated hops. Numerically, this forces the quantum populations to follow the classical populations and the simulation remains internally consistent. While the concept of frustrated hops does not exist for MCE or AIMC, for SH the frustrated hops are prevented and no change is made to the nuclear velocities.

The AIMC implementation in NEXMD directly follows the algorithm described in ref 20, with the exception of the third cloning criterion, which is replaced here with the sum of all Tully's FSSH hopping probabilities (eq 4)[10] from the most populated electronic state (largest instantaneous $|c_a|$) divided by the time step. This has the advantage of introducing the velocity into the criterion, which scales the nonadiabatic coupling. The maximum number of cloning events was set to 16 and the cloning criteria thresholds were 1.5 (first criterion), 5° (second criterion), and 0.05 (third criterion). The AIMC cloning process is performed on-the-fly with additional clones propagating concurrently with their "parents". This is feasible (in a serial propagation) only because of the highly efficient semiempirical electronic structure representation. So far, post processing is required for MCE propagation of clones after the main run. Simulations of large systems or simulations using more computationally expensive electronic structure techniques may require multiple runs, which may favor postprocessing approaches and independent trajectories. However, for applicable systems, a more advanced and convenient on-the-fly MCE function, which avoids post processing and reduces disk-space requirements, is tested in NWChem[59] (based on the TDDFT framework). This approach will also be implemented in NEXMD in the future. For the Gaussian width α (eq 6), we use the average atom-dependent width parameters given by Thompson *et al.*[78] of 4.7 and 22.7 $Bohr^{-2}$ for hydrogen and carbon, respectively. As shown here, the AIMC results are largely insensitive to scaling around these values for realistic molecular systems.

ASSOCIATED CONTENT

Supporting Information

The Supporting Information is available free of charge at https://pubs.acs.org/doi/10.1021/acs.jpclett.1c00266.

Transition densities showing the number of excited states included in the nonadiabatic dynamics and the initial state for each system; AIMC simulation parameters used to generate data plotted in Figure 5; plots of relative differences between adiabatic state populations obtained from EHR and AIMC simulations using different parameters compared to our most accurate AIMC results (PDF)

AUTHOR INFORMATION

Corresponding Authors

Sebastian Fernandez-Alberti − *Universidad Nacional de Quilmes, B1876BXD Bernal, Argentina;* orcid.org/0000-0002-0916-5069; Email: sfalberti@gmail.com

Sergei Tretiak − *Theoretical Division, Los Alamos National Laboratory, Los Alamos, New Mexico 87545, United States;* orcid.org/0000-0001-5547-3647; Email: serg@lanl.gov

https://doi.org/10.1021/acs.jpclett.1c00266
J. Phys. Chem. Lett. 2021, 12, 2970−2982

Authors

Victor M. Freixas − *Universidad Nacional de Quilmes, B1876BXD Bernal, Argentina;* orcid.org/0000-0003-1733-4827

Alexander J. White − *Theoretical Division, Los Alamos National Laboratory, Los Alamos, New Mexico 87545, United States;* orcid.org/0000-0002-7771-3899

Tammie Nelson − *Theoretical Division, Los Alamos National Laboratory, Los Alamos, New Mexico 87545, United States;* orcid.org/0000-0002-3173-5291

Huajing Song − *Theoretical Division, Los Alamos National Laboratory, Los Alamos, New Mexico 87545, United States;* orcid.org/0000-0001-5958-7377

Dmitry V. Makhov − *School of Chemistry, University of Leeds, Leeds LS2 9JT, U.K.; School of Mathematics, University of Bristol, Bristol BS8 1TW, U.K.*

Dmitrii Shalashilin − *School of Chemistry, University of Leeds, Leeds LS2 9JT, U.K.;* orcid.org/0000-0001-6104-1277

Complete contact information is available at: https://pubs.acs.org/10.1021/acs.jpclett.1c00266

Notes

The authors declare no competing financial interest.

■ ACKNOWLEDGMENTS

The work at Los Alamos National Laboratory (LANL) was supported by the LANL Directed Research and Development Funds (LDRD) and performed in part at the Center for Nonlinear Studies (CNLS) and the Center for Integrated Nanotechnologies (CINT), a U.S. Department of Energy, Office of Science user facility at LANL. This research used resources provided by the LANL Institutional Computing (IC) Program. H.S. and S.T. acknowledge support from the U.S. DOE, Office of Science, Basic Energy Sciences, Chemical Sciences, Geosciences, and Biosciences Division under Contract No. KC0301030. S.F.-A. and V.M.F. were supported by CONICET, UNQ, and ANPCyT (Grant No. PICT-2018-02360). D.V.M. and D.S. acknowledge EPSRC Grant EP/P021123/1. LANL is operated by Triad National Security, LLC, for the U.S. Department of Energy National Nuclear Security Administration under Contract No. 89233218CNA000001.

■ REFERENCES

(1) Scholes, G. D.; Fleming, G. R.; Olaya-Castro, A.; van Grondelle, R. Lessons from Nature About Solar Light Harvesting. *Nat. Chem.* **2011**, *3*, 763−774.

(2) Burroughes, J. H.; Bradley, D. D. C.; Brown, A. R.; Marks, R. N.; Mackay, K.; Friend, R. H.; Burns, P. L.; Holmes, A. B. Light-Emitting Diodes Based on Conjugated Polymers. *Nature* **1990**, *347*, 539−541.

(3) Akimov, A. V.; Neukirch, A. J.; Prezhdo, O. V. Theoretical Insights into Photoinduced Charge Transfer and Catalysis at Oxide Interfaces. *Chem. Rev.* **2013**, *113*, 4496−4565.

(4) Schroeder, V.; Savagatrup, S.; He, M.; Lin, S.; Swager, T. M. Carbon Nanotube Chemical Sensors. *Chem. Rev.* **2019**, *119*, 599−663.

(5) Spano, F. C. The Spectral Signatures of Frenkel Polarons in H- and J-Aggregates. *Acc. Chem. Res.* **2010**, *43*, 429−439.

(6) Scholes, G. D.; Rumbles, G. Excitons in Nanoscale Systems. *Nat. Mater.* **2006**, *5*, 683−696.

(7) Mukamel, S.; Abramavicius, D.; Yang, L.; Zhuang, W.; Schweigert, I. V.; Voronine, D. V. Coherent Multidimensional Optical Probes for Electron Correlations and Exciton Dynamics: From Nmr to X-Rays. *Acc. Chem. Res.* **2009**, *42*, 553−562.

(8) Marangos, J. P. Accessing the Quantum Spatial and Temporal Scales with Xfels. *Nat. Rev. Phys.* **2020**, *2*, 332−334.

(9) Schuurman, M. S.; Stolow, A. Dynamics at Conical Intersections. *Annu. Rev. Phys. Chem.* **2018**, *69*, 427−450.

(10) Tully, J. C. Molecular Dynamics with Electronic Transitions. *J. Chem. Phys.* **1990**, *93*, 1061−1071.

(11) Ehrenfest, P. Bemerkung Uber Die Angenaherte Gultigkeit Der Klassischen Mechanik Innerhalb Der Quantenmechanik. *Eur. Phys. J. A* **1927**, *45*, 455−457.

(12) Crespo-Otero, R.; Barbatti, M. Recent Advances and Perspectives on Nonadiabatic Mixed Quantum-Classical Dynamics. *Chem. Rev.* **2018**, *118*, 7026−7068.

(13) Nelson, T. R.; White, A. J.; Bjorgaard, J. A.; Sifain, A. E.; Zhang, Y.; Nebgen, B.; Fernandez-Alberti, S.; Mozyrsky, D.; Roitberg, A. E.; Tretiak, S. Non-Adiabatic Excited-State Molecular Dynamics: Theory and Applications for Modeling Photophysics in Extended Molecular Materials. *Chem. Rev.* **2020**, *120*, 2215−2287.

(14) Curchod, B. F. E.; Martínez, T. J. Ab Initio Nonadiabatic Quantum Molecular Dynamics. *Chem. Rev.* **2018**, *118*, 3305−3336.

(15) Worth, G. A.; Meyer, H. D.; Köppel, H.; Cederbaum, L. S.; Burghardt, I. Using the Mctdh Wavepacket Propagation Method to Describe Multimode Non-Adiabatic Dynamics. *Int. Rev. Phys. Chem.* **2008**, *27*, 569−606.

(16) Mai, S.; Marquetand, P.; González, L. Surface Hopping Molecular Dynamics. In *Quantum Chemistry and Dynamics of Excited States*; 2020; pp 499−530.

(17) Ben-Nun, M.; Quenneville, J.; Martínez, T. J. Ab Initio Multiple Spawning: Photochemistry from First Principles Quantum Molecular Dynamics. *J. Phys. Chem. A* **2000**, *104*, 5161−5175.

(18) Makhov, D. V.; Glover, W. J.; Martínez, T. J.; Shalashilin, D. V. Ab Initio Multiple Cloning Algorithm for Quantum Nonadiabatic Molecular Dynamics. *J. Chem. Phys.* **2014**, *141*, No. 054110.

(19) Fernandez-Alberti, S.; Makhov, D. V.; Tretiak, S.; Shalashilin, D. V. Non-Adiabatic Excited State Molecular Dynamics of Phenylene Ethynylene Dendrimer Using a Multiconfigurational Ehrenfest Approach. *Phys. Chem. Chem. Phys.* **2016**, *18*, 10028−10040.

(20) Freixas, V. M.; Fernandez-Alberti, S.; Makhov, D. V.; Tretiak, S.; Shalashilin, D. An Ab Initio Multiple Cloning Approach for the Simulation of Photoinduced Dynamics in Conjugated Molecules. *Phys. Chem. Chem. Phys.* **2018**, *20*, 17762−17772.

(21) Subotnik, J. E.; Jain, A.; Landry, B.; Petit, A.; Ouyang, W.; Bellonzi, N. Understanding the Surface Hopping View of Electronic Transitions and Decoherence. *Annu. Rev. Phys. Chem.* **2016**, *67*, 387−417.

(22) Wang, L.; Akimov, A.; Prezhdo, O. V. Recent Progress in Surface Hopping: 2011−2015. *J. Phys. Chem. Lett.* **2016**, *7*, 2100−2112.

(23) Ibele, L. M.; Curchod, B. F. E. A Molecular Perspective on Tully Models for Nonadiabatic Dynamics. *Phys. Chem. Chem. Phys.* **2020**, *22*, 15183−15196.

(24) Dewar, M. J. S.; Zoebisch, E. G.; Healy, E. F.; Stewart, J. J. P. Development and Use of Quantum Mechanical Molecular Models. 76. Am1: A New General Purpose Quantum Mechanical Molecular Model. *J. Am. Chem. Soc.* **1985**, *107*, 3902−3909.

(25) Malone, W.; et al. Nexmd Software Package for Nonadiabatic Excited State Molecular Dynamics Simulations. *J. Chem. Theory Comput.* **2020**, *16*, 5771−5783.

(26) Barbatti, M.; Sen, K. Effects of Different Initial Condition Samplings on Photodynamics and Spectrum of Pyrrole. *Int. J. Quantum Chem.* **2016**, *116*, 762−771.

(27) Makhov, D. V.; Saita, K.; Martínez, T. J.; Shalashilin, D. V. Ab Initio Multiple Cloning Simulations of Pyrrole Photodissociation: Tker Spectra and Velocity Map Imaging. *Phys. Chem. Chem. Phys.* **2015**, *17*, 3316−3325.

(28) Alonso, J. L.; Bruscolini, P.; Castro, A.; Clemente-Gallardo, J.; Cuchí, J. C.; Jover-Galtier, J. A. Ehrenfest Statistical Dynamics in Chemistry: Study of Decoherence Effects. *J. Chem. Theory Comput.* **2018**, *14*, 3975−3985.

(29) Subotnik, J. E. Augmented Ehrenfest Dynamics Yields a Rate for Surface Hopping. *J. Chem. Phys.* **2010**, *132*, 134112.
(30) Nijjar, P.; Jankowska, J.; Prezhdo, O. V. Ehrenfest and Classical Path Dynamics with Decoherence and Detailed Balance. *J. Chem. Phys.* **2019**, *150*, 204124.
(31) Esch, M. P.; Levine, B. G. Decoherence-Corrected Ehrenfest Molecular Dynamics on Many Electronic States. *J. Chem. Phys.* **2020**, *153*, 114104.
(32) Jasper, A. W.; Truhlar, D. G. Improved Treatment of Momentum at Classically Forbidden Electronic Transitions in Trajectory Surface Hopping Calculations. *Chem. Phys. Lett.* **2003**, *369*, 60−67.
(33) Martens, C. C. Surface Hopping by Consensus. *J. Phys. Chem. Lett.* **2016**, *7*, 2610−2615.
(34) Sifain, A. E.; Wang, L.; Prezhdo, O. V. Mixed Quantum-Classical Equilibrium in Global Flux Surface Hopping. *J. Chem. Phys.* **2015**, *142*, 224102.
(35) Fernandez-Alberti, S.; Roitberg, A. E.; Nelson, T.; Tretiak, S. Identification of Unavoided Crossings in Nonadiabatic Photoexcited Dynamics Involving Multiple Electronic States in Polyatomic Conjugated Molecules. *J. Chem. Phys.* **2012**, *137*, No. 014512.
(36) Ghosh, S.; Giannini, S.; Lively, K.; Blumberger, J. Nonadiabatic Dynamics with Quantum Nuclei: Simulating Charge Transfer with Ring Polymer Surface Hopping. *Faraday Discuss.* **2020**, *221*, 501−525.
(37) Jaeger, H. M.; Fischer, S.; Prezhdo, O. V. Decoherence-Induced Surface Hopping. *J. Chem. Phys.* **2012**, *137*, 22A545.
(38) Nelson, T.; Fernandez-Alberti, S.; Roitberg, A. E.; Tretiak, S. Nonadiabatic Excited-State Molecular Dynamics: Treatment of Electronic Decoherence. *J. Chem. Phys.* **2013**, *138*, 224111.
(39) Zhu, C.; Nangia, S.; Jasper, A. W.; Truhlar, D. G. Coherent Switching with Decay of Mixing: An Improved Treatment of Electronic Coherence for Non-Born-Oppenheimer Trajectories. *J. Chem. Phys.* **2004**, *121*, 7658−7670.
(40) Symonds, C.; Kattirtzi, J. A.; Shalashilin, D. V. The Effect of Sampling Techniques Used in the Multiconfigurational Ehrenfest Method. *J. Chem. Phys.* **2018**, *148*, 184113.
(41) Shalashilin, D. V.; Child, M. S. The Phase Space Ccs Approach to Quantum and Semiclassical Molecular Dynamics for High-Dimensional Systems. *Chem. Phys.* **2004**, *304*, 103−120.
(42) Joubert-Doriol, L.; Sivasubramanium, J.; Ryabinkin, I. G.; Izmaylov, A. F. Topologically Correct Quantum Nonadiabatic Formalism for on-the-Fly Dynamics. *J. Phys. Chem. Lett.* **2017**, *8*, 452−456.
(43) Heller, E. J. Time-Dependent Approach to Semiclassical Dynamics. *J. Chem. Phys.* **1975**, *62*, 1544−1555.
(44) Mignolet, B.; Curchod, B. F. E. A Walk through the Approximations of Ab Initio Multiple Spawning. *J. Chem. Phys.* **2018**, *148*, 134110.
(45) Ben-Nun, M.; Martínez, T. J. Ab Initio Quantum Molecular Dynamics. *Adv. Chem. Phys.* **2002**, *121*, 439−512.
(46) Segatta, F.; Cupellini, L.; Garavelli, M.; Mennucci, B. Quantum Chemical Modeling of the Photoinduced Activity of Multichromophoric Biosystems. *Chem. Rev.* **2019**, *119*, 9361−9380.
(47) Nelson, T.; Fernandez-Alberti, S.; Roitberg, A. E.; Tretiak, S. Nonadiabatic Excited-State Molecular Dynamics: Modeling Photophysics in Organic Conjugated Materials. *Acc. Chem. Res.* **2014**, *47*, 1155−1164.
(48) Sifain, A. E.; et al. Photoexcited Nonadiabatic Dynamics of Solvated Push−Pull Π-Conjugated Oligomers with the Nexmd Software. *J. Chem. Theory Comput.* **2018**, *14*, 3955−3966.
(49) Giannini, S.; Carof, A.; Ellis, M.; Yang, H.; Ziogos, O. G.; Ghosh, S.; Blumberger, J. Quantum Localization and Delocalization of Charge Carriers in Organic Semiconducting Crystals. *Nat. Commun.* **2019**, *10*, 3843.
(50) Heck, A.; Kranz, J. J.; Kubař, T.; Elstner, M. Multi-Scale Approach to Non-Adiabatic Charge Transport in High-Mobility Organic Semiconductors. *J. Chem. Theory Comput.* **2015**, *11*, 5068−5082.
(51) Wang, L.; Beljonne, D. Flexible Surface Hopping Approach to Model the Crossover from Hopping to Band-Like Transport in Organic Crystals. *J. Phys. Chem. Lett.* **2013**, *4*, 1888−1894.
(52) Barbatti, M.; Ruckenbauer, M.; Plasser, F.; Pittner, J.; Granucci, G.; Persico, M.; Lischka, H. Newton-X: A Surface-Hopping Program for Nonadiabatic Molecular Dynamics. *WIREs Comput. Mol. Sci.* **2014**, *4*, 26−33.
(53) Richter, M.; Marquetand, P.; González-Vázquez, J.; Sola, I.; González, L. Sharc: Ab Initio Molecular Dynamics with Surface Hopping in the Adiabatic Representation Including Arbitrary Couplings. *J. Chem. Theory Comput.* **2011**, *7*, 1253−1258.
(54) Akimov, A. V.; Prezhdo, O. V. Advanced Capabilities of the Pyxaid Program: Integration Schemes, Decoherence Effects, Multi-excitonic States, and Field-Matter Interaction. *J. Chem. Theory Comput.* **2014**, *10*, 789−804.
(55) Case, D.; et al. *Amber 2017*; University of California: San Francisco, 2017.
(56) Nelson, T.; Fernandez-Alberti, S.; Chernyak, V.; Roitberg, A. E.; Tretiak, S. Nonadiabatic Excited-State Molecular Dynamics Modeling of Photoinduced Dynamics in Conjugated Molecules. *J. Phys. Chem. B* **2011**, *115*, 5402−5414.
(57) Paterlini, M. G.; Ferguson, D. M. Constant Temperature Simulations Using the Langevin Equation with Velocity Verlet Integration. *Chem. Phys.* **1998**, *236*, 243−252.
(58) Song, H.; Fischer, S. A.; Zhang, Y.; Cramer, C. J.; Mukamel, S.; Govind, N.; Tretiak, S. First Principles Nonadiabatic Excited-State Molecular Dynamics in Nwchem. *J. Chem. Theory Comput.* **2020**, *16*, 6418−6427.
(59) Song, H.; Freixas, V. M.; Fernandez-Alberti, S.; White, A. J.; Zhang, Y.; Mukamel, S.; Govind, N.; Tretiak, S. First Principles an Ab Initio Multiple Cloning Method for Excited-State Molecular Dynamics in Nwchem. *J. Chem. Theory. Comput.* **2021**, submitted for publication.
(60) Freixas, V. M.; Tretiak, S.; Makhov, D. V.; Shalashilin, D. V.; Fernandez-Alberti, S. Vibronic Quantum Beating between Electronic Excited States in a Heterodimer. *J. Phys. Chem. B* **2020**, *124*, 3992−4001.
(61) Andrews, D. L. Light Harvesting in Dendrimer Materials: Designer Photophysics and Electrodynamics. *J. Mater. Res.* **2012**, *27*, 627−638.
(62) Magyar, R. J.; Tretiak, S.; Gao, Y.; Wang, H. L.; Shreve, A. P. A Joint Theoretical and Experimental Study of Phenylene−Acetylene Molecular Wires. *Chem. Phys. Lett.* **2005**, *401*, 149−156.
(63) Swallen, S. F.; Zhu, Z.; Moore, J. S.; Kopelman, R. Correlated Excimer Formation and Molecular Rotational Dynamics in Phenylacetylene Dendrimers. *J. Phys. Chem. B* **2000**, *104*, 3988−3995.
(64) Ondarse-Alvarez, D.; Oldani, N.; Roitberg, A. E.; Kleiman, V.; Tretiak, S.; Fernandez-Alberti, S. Energy Transfer and Spatial Scrambling of an Exciton in a Conjugated Dendrimer. *Phys. Chem. Chem. Phys.* **2018**, *20*, 29648−29660.
(65) Kleiman, V. D.; Melinger, J. S.; McMorrow, D. Ultrafast Dynamics of Electronic Excitations in a Light-Harvesting Phenylacetylene Dendrimer. *J. Phys. Chem. B* **2001**, *105*, 5595−5598.
(66) Fernandez-Alberti, S.; Roitberg, A. E.; Kleiman, V. D.; Nelson, T.; Tretiak, S. Shishiodoshi Unidirectional Energy Transfer Mechanism in Phenylene Ethynylene Dendrimers. *J. Chem. Phys.* **2012**, *137*, 22A526.
(67) Freixas, V. M.; Ondarse-Alvarez, D.; Tretiak, S.; Makhov, D. V.; Shalashilin, D. V.; Fernandez-Alberti, S. Photoinduced Non-Adiabatic Energy Transfer Pathways in Dendrimer Building Blocks. *J. Chem. Phys.* **2019**, *150*, 124301.
(68) Nishioka, K.; Suzuki, M. Dynamics of Unidirectional Exciton Migration to the Molecular Periphery in a Photoexcited Compact Dendrimer. *J. Chem. Phys.* **2005**, *122*, No. 024708.
(69) Barford, W. *Electronic and Optical Properties of Conjugated Polymers*; Oxford University Press: Oxford, UK, 2013.
(70) Galindo, J. F.; Atas, E.; Altan, A.; Kuroda, D. G.; Fernandez-Alberti, S.; Tretiak, S.; Roitberg, A. E.; Kleiman, V. D. Dynamics of Energy Transfer in a Conjugated Dendrimer Driven by Ultrafast

https://doi.org/10.1021/acs.jpclett.1c00266
J. Phys. Chem. Lett. 2021, 12, 2970−2982

Localization of Excitations. *J. Am. Chem. Soc.* **2015**, *137*, 11637−11644.
(71) Ondarse-Alvarez, D.; Komurlu, S.; Roitberg, A. E.; Pierdominici-Sottile, G.; Tretiak, S.; Fernandez-Alberti, S.; Kleiman, V. D. Ultrafast Electronic Energy Relaxation in a Conjugated Dendrimer Leading to Inter-Branch Energy Redistribution. *Phys. Chem. Chem. Phys.* **2016**, *18*, 25080−25089.
(72) Nelson, T.; Fernandez-Alberti, S.; Roitberg, A. E.; Tretiak, S. Conformational Disorder in Energy Transfer: Beyond Forster Theory. *Phys. Chem. Chem. Phys.* **2013**, *15*, 9245−9256.
(73) Becker, K.; Da Como, E.; Feldmann, J.; Scheliga, F.; Thorn Csányi, E.; Tretiak, S.; Lupton, J. M. How Chromophore Shape Determines the Spectroscopy of Phenylene−Vinylenes: Origin of Spectral Broadening in the Absence of Aggregation. *J. Phys. Chem. B* **2008**, *112*, 4859−4864.
(74) Tretiak, S.; Zhang, W. M.; Chernyak, V.; Mukamel, S. Excitonic Couplings and Electronic Coherence in Bridged Naphthalene Dimers. *Proc. Natl. Acad. Sci. U. S. A.* **1999**, *96*, 13003.
(75) Keefer, D.; Freixas, V. M.; Song, H.; Tretiak, S.; Fernandez-Alberti, S.; Mukamel, S. Probing Intramolecular Vibronic Coherences in Complex Molecules by Ultrafast Stimulated X-Ray Raman Signals. *Chem. Sci.* **2021**, submitted for publication.
(76) Nelson, T. R.; Ondarse-Alvarez, D.; Oldani, N.; Rodriguez-Hernandez, B.; Alfonso-Hernandez, L.; Galindo, J. F.; Kleiman, V. D.; Fernandez-Alberti, S.; Roitberg, A. E.; Tretiak, S. Coherent Exciton-Vibrational Dynamics and Energy Transfer in Conjugated Organics. *Nat. Commun.* **2018**, *9*, 2316.
(77) Chernyak, V.; Mukamel, S. Density-Matrix Representation of Nonadiabatic Couplings in Time-Dependent Density Functional (Tddft) Theories. *J. Chem. Phys.* **2000**, *112*, 3572−3579.
(78) Thompson, A. L.; Punwong, C.; Martínez, T. J. Optimization of Width Parameters for Quantum Dynamics with Frozen Gaussian Basis Sets. *Chem. Phys.* **2010**, *370*, 70−77.
(79) Miao, G.; Subotnik, J. Revisiting the Recoherence Problem in the Fewest Switches Surface Hopping Algorithm. *J. Phys. Chem. A* **2019**, *123*, 5428−5435.
(80) Zhu, C. Restoring Electronic Coherence/Decoherence for a Trajectory-Based Nonadiabatic Molecular Dynamics. *Sci. Rep.* **2016**, *6*, 24198.
(81) Fischer, S. A.; Chapman, C. T.; Li, X. Surface Hopping with Ehrenfest Excited Potential. *J. Chem. Phys.* **2011**, *135*, 144102.

https://doi.org/10.1021/acs.jpclett.1c00266
J. Phys. Chem. Lett. 2021, 12, 2970−2982